



# Evaluation of mechanical properties characterization of additively manufactured components

Felix Frölich<sup>1</sup> · Lennart Bechtloff<sup>1,2</sup> · Benedikt M. Scheuring<sup>2</sup> · Anselm L. Heuer<sup>2</sup> · Florian Wittemann<sup>1</sup> · Luise Kärger<sup>1</sup> · Wilfried V. Liebig<sup>2</sup>

Received: 1 February 2024 / Accepted: 27 May 2024  
© The Author(s) 2024

## Abstract

Additive manufacturing by material extrusion offers innovative potential for component design and is driving advances in many industries. However, fully harnessing these advancements necessitates a thorough comprehension of the process-specific anisotropic structural properties. The complex interactions between process parameters and their direct influence on structural properties often lead to discrepancies between the mechanical properties of tested specimens at the coupon level and the inherent properties of additively manufactured components. In addition, there is no standardized method for preparing specimens that represent the mechanical properties within a given component. This further complicates the comparison of measured properties of different series of measurements and the investigation of manufacturing effects that may occur during the production of a component. Given these challenges, the present work addresses the fundamental question of what aspects need to be considered to ensure that the test specimens reflect the process conditions being tested. The studies look at the requirements for producing representative specimens and for the test methodology to characterize the mechanical properties of additively manufactured structures. The tests are carried out on specimens that were produced directly using the material extrusion process and on specimens that were cut from additively manufactured plates. Water jet cutting, milling, and laser cutting are investigated and compared as cutting methods. The influence of the specimen geometry and the size of the additively manufactured plate is considered. The orientation-dependent mechanical properties, the significance of the individual tests, the measurement scatter, and scanning electron micrographs of the cut edges and fracture surfaces are analyzed. Finally, guidelines for performing representative tests to characterize the mechanical properties of additively manufactured components are proposed.

**Keywords** Additive manufacturing · Material extrusion (MEX) · Fused filament fabrication (FFF) · Fused deposition modeling (FDM) · Mechanical characterization

---

✉ Felix Frölich  
felix.froelich@kit.edu

Lennart Bechtloff  
uexuf@student.kit.edu

Benedikt M. Scheuring  
benedikt.scheuring@kit.edu

Anselm L. Heuer  
anselm.heuer@kit.edu

Florian Wittemann  
florian.wittemann@kit.edu

Luise Kärger  
luise.kaerger@kit.edu

Wilfried V. Liebig  
wilfried.liebig@kit.edu

<sup>1</sup> Institute of Vehicle System Technology - Lightweight Engineering, Karlsruhe Institute of Technology (KIT), Rintheimer Querallee 2, 76131 Karlsruhe, Baden-Württemberg, Germany

<sup>2</sup> Institute for Applied Materials - Materials Science and Engineering, Karlsruhe Institute of Technology (KIT), Engelbert-Arnold-Straße 4, 76131 Karlsruhe, Baden-Württemberg, Germany

## 1 Introduction

Additive manufacturing (AM) processes have established themselves as part of the continuous development of component design methods due to their numerous advantages. These include the direct and cost-effective production of complex geometries, individual design options, and low material consumption [1, 2]. This paper addresses one specific AM technology, namely material extrusion (MEX). When the feedstock within MEX is a thermoplastic filament, then the process is known as Fused Filament Fabrication (FFF) and has been commercialized under the name Fused Deposition Modeling (FDM) [3]. So far, it has been used mainly for consumer applications and prototyping. Ongoing process improvements and the reusability of materials are expanding its applicability in many industries. However, the potential of additively manufactured polymer-based structures has not yet been fully exploited due to their complex deformation and failure behavior [4–10]. This is due to the intrinsic heterogeneity of the structures [11–13]. The process-related layer structure and the deposition strategy within the layers in different paths lead to this heterogeneity [14] and thus have an effect on the mechanical behavior [6, 15–17]: Reduced interfacial strength between individual strands, but also between layers [18, 19], pores between strands [20], different orientation of deposited strands concerning the load direction, and increased surface waviness due to the shape of the strand. Figure 1 shows these structural features within the additive structure. The characteristic triangular (I) and diamond-shaped (II) voids between the layers are shown. Figure 2 shows a microscopic image of the FFF structure studied in this work. The oval shape of the strands and the shaped interfaces are visible. There is a large

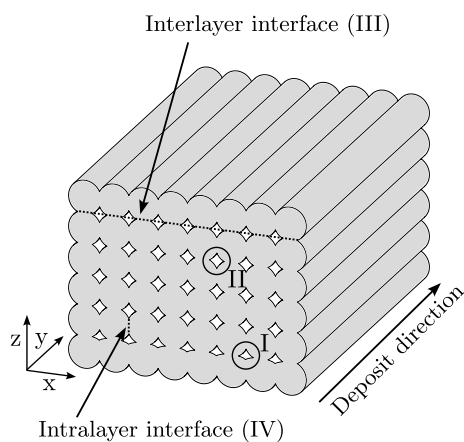


**Fig. 1** Structural features and their position within the additive structure. Characteristic triangular (I), diamond-shaped (II) cavities between the layers, the interlayer bonding interfaces (III), and the intralayer bonding interfaces (IV) are shown

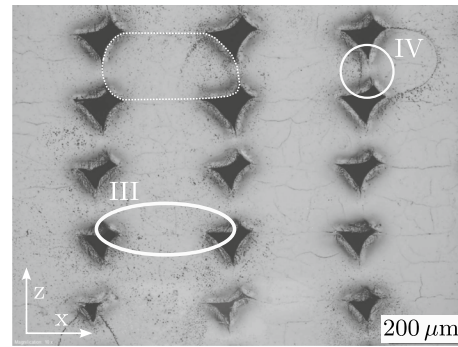


**Fig. 2** Microscopic image of the FFF structure investigated in this work. There is a large neck formation between the layers, the interlayer bonding interfaces (III), and a small neck formation between adjacent strands within the layers, the intralayer bonding interfaces (IV)

neck formation between the layers, the interlayer bonding interfaces (III), and a small neck formation within the layers, the intralayer bonding interfaces (IV). These different bonding interfaces are also shown in Fig. 1.

Already in the early 2000 s, the structure–property relation of some of these properties was investigated in more detail. For example, EsSaid et al. [14] and Ahn et al. [21] have shown a dependence of both strength and stiffness on the orientation of the deposited strands. In addition, a relationship between the number of pores and the strength or stiffness was demonstrated. Cuan-Urquiza et al. [6] summarized the previous research on the structure–property relationships of these features in their 2019 review article. The study of the various influences of structural features requires an appropriate characterization method. Cuan-Urquiza et al. [6] even defines the selected characterization method itself as an influencing parameter. First, different specimen geometries can be distinguished. For example, both a dogbone and a rectangle shape allow the investigation of mechanical parameters. For characterization in the injection molding process, standards such as DIN EN ISO 527-2 [22] for testing tensile properties using dogbone specimens are available. However, these standards do not define how the specimens should be produced in polymer-based AM. Cuan-Urquiza et al. [6] show, for example, that if the specimens are printed directly in the corresponding geometry, the perimeter and turning points of the nozzle trajectory influence the effective orientation in the measuring range of the specimen. For small specimens, this can lead to the methodological error that, despite the desired 90° orientation of the strands to the loading direction, there is no pure 90° orientation. In addition, pores formed at the turning points between the perimeter and the filling lead to an additional internal notch effect [20]. If the ratio of specimen width to strand width is not an integer, other geometrically induced pores and notch effects may occur. These influences may explain the different

tensile strengths of two specimen shapes (ASTM D638-14 Type I and Type IV) that Laureto and Pearce [23] observed in a large-scale measurement campaign. When the specimens are examined after specimen post-processing, further differences become apparent. Zhang et al. [24] used water jet cutting to cut specimens from additively manufactured plates and showed that both the stiffness and strength of the cut specimens were on average 50 % lower than those of the directly manufactured specimens. This was explained by the absence of perimeters, which have a strengthening effect in the load direction. In contrast, the cut specimens failed more often within the measurement length due to the lack of process-related notches in the conical area. This increase in validity was also observed from Park et al. [25], where the validity increased from about 27 % to 62 %. Validity was also assessed based on the crack initiation point. Park et al. [25] uses a laser cutter for specimen preparation. The literature shows that the methods used to characterize additively manufactured structures and the specimen preparation have a significant influence on the measured mechanical properties. However, there is a lack of standardized approaches, making it difficult to compare results and use them as a reference for further research. The motivation for this work is to address this problem. The research aims to address the fundamental question of what factors are essential to ensure that test specimens accurately reflect the process conditions being evaluated. Building on preliminary investigations published in previous publications [26], this study aims to establish guidelines for specimen preparation. These guidelines are designed to ensure that measurements not only accurately capture the inherent structure under investigation but also provide highly reproducible results. Initial results of the authors [26] will be further discussed, and additional experimental investigations will be carried out. The first step is to formulate requirements for the test specimen itself, and then to formulate hypotheses on how these requirements can be met. It is investigated whether there is a significant difference in the measured properties when the test specimens are separated from a printed plate or directly printed. As part of the first preparation method, the two geometries dogbone and rectangle are also compared. These are additionally prepared with three different intralayer orientations  $0^\circ$ ,  $90^\circ$ , and  $\pm 45^\circ$  to the load direction. In addition, different cutting methods are investigated to assess their influence on the measurements. The different preparation methods are evaluated based on the intralayer orientation-dependent mechanical properties, the validity of the individual experiments, the size of the measurement deviations, and scanning electron micrographs of the cut edges and fracture surfaces. Based on these investigations, guidelines for specimen preparation are derived and data to be provided are identified to enable reproducible investigation of the characteristic properties of additively manufactured structures.

**Table 1** Material properties of BASF Ultrafuse PLA filament [27]

Process parameter	Value	Unit
Density $\rho$	1248	kg m <sup>-3</sup>
Glass transition temperature $T_G$	60	°C
Melting temperature $T_M$	151	°C
Processing temperature $T_{proc}$	210–230	°C

**Table 2** Slicer and process parameters selected for the manufacturing of all specimens

Process parameter	Value	Unit
Nozzle temperature $T_N$	210	°C
Bed temperature $T_{bed}$	60	°C
Layer height $l_{height}$	0.2	mm
Extrusion width $e_{width}$	0.4	mm
Infill printing speed $v_{infill}$	50	mm s <sup>-1</sup>
Perimeter printing speed $v_{peri}$	40	mm s <sup>-1</sup>
Flow rate (Slicer) $V_{poly}$	95	%
Maximum acceleration $a_{max}$	750	mm s <sup>-2</sup>

## 2 Material manufacturing and characterization method

### 2.1 Materials

The material used is the commercial Ultrafuse polylactic acid (PLA) filament from BASF [27]. Its low melting and glass transition temperatures, low tendency to warp, and relatively high surface hardness make it particularly suitable for AM, allowing robust process control [28]. Owing to its good printability, PLA has been used exemplary in this work. The low susceptibility to distortion and defects facilitates the systematic investigation of differently manufactured specimens. The following material properties, shown in Table 1, are specified in [27].

### 2.2 Process parameters

The *Ultimaker 2+* from the company *Ultimaker* was used to produce the test specimens in this work. According to the manufacturer, the positioning accuracy in the  $x$ - $y$  plane of the print bed is 25.5  $\mu\text{m}$ , in the  $z$ -axis 5  $\mu\text{m}$ . The *Ultimaker 2+* has a heatable printing bed. The standard glass printing bed was replaced with the *FilaPrint* permanent printing bed. The nozzle used has a diameter of 0.4 mm and was specified with a print resolution of 200  $\mu\text{m}$  to 20  $\mu\text{m}$ . The printing bed was leveled using three adjusting screws. The slicer and printer settings listed in Table 2

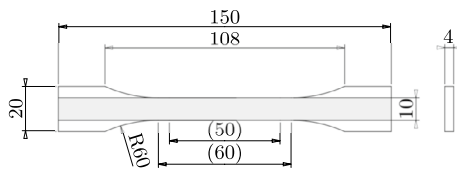


**Fig. 3** Dimensions for a dogbone and rectangular specimen shape in mm according to DIN EN ISO 527-2 [22]

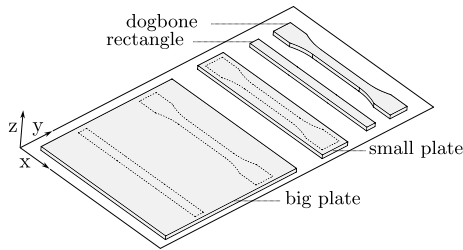


**Fig. 4** Illustration of the different ways of preparing the specimens to be tested. Directly printed and cut from plates of different sizes

were selected based on printing studies to achieve a consistent and reproducible microstructure. The fan was turned on from the second layer.

### 2.3 Specimen geometry

In this study, experimental investigations were conducted on test specimens with a dogbone geometry and rectangular shape, following DIN EN ISO 527-2 standards as illustrated in Fig. 3.

### 2.4 Specimen preparation

PLA structures with 100% fill density and varying intra-layer material orientations are printed. This includes unidirectional structures oriented along the load direction ( $0^\circ$ ), structures oriented transverse to the load direction ( $90^\circ$ ), and structures with alternating material orientations of  $\pm 45^\circ$ . Each preparation configuration undergoes a minimum of five valid tests for evaluation. To investigate the mechanical properties and failure behavior of direct printed specimens,

**Table 3** Minimum plate sizes, dimensioned using Eq. 1, the process parameters listed in Table 2, the specified specimen dimensions, the number of specimens and the cutting width for cutting

Plate type	Dimensions $x$ - $y$ in mm		
	$\alpha = 0^\circ$	$\alpha = 90^\circ$	$\alpha = \pm 45^\circ$
Large	$155 \times 122$	$152 \times 125$	$154 \times 124$
Small	$155 \times 22$	$152 \times 25$	$154 \times 24$

both dogbone and rectangular specimens are fabricated using the process parameters detailed in Table 2. All direct printed specimens are printed with a perimeter.

To compare directly additively manufactured test specimens with specimens cut from additively manufactured plates, large square plates were utilized. Five specimens were cut from each square plate by water jet cutting. Additionally, small rectangular plates were produced to accommodate exactly one dogbone specimen, allowing for an assessment of the effect of plate size. Figure 4 provides an overview of the specimen variants.

Finally, specimens were cut from the smaller plates using various cutting methods to quantify the influence of the cutting method on the mechanical properties.

### 2.5 Plate dimensions

In addition to the material allowance due to the cutting method, an additional distance  $d_{edge}$  at the edges of the plate (see Fig. 5) must be considered when dimensioning the plates. This is crucial due to the printer-specific acceleration after changing the extrusion direction and the perimeter. It ensures that the resulting print velocity in the test area of the specimen matches the velocity set in the slicer, as illustrated in Fig. 5 and previously discussed in [26], confirming hypothesis H 1. The additional distance  $d_{edge}$  on each edge of the plate can be estimated by

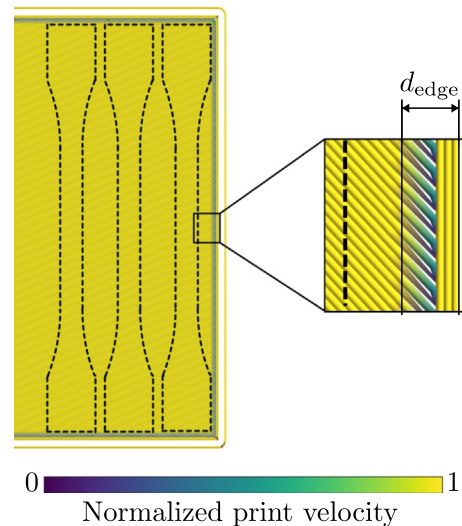


**Fig. 5** Resulting nozzle velocity  $v_{nozzle}$ , normalized to the specified infill velocity  $v_{infill}$ , considers hardware limitations such as acceleration and possible curve velocities. This calculation and visualization are performed using the Python package PyGodeDecode [29]. The additional required width  $d_{edge}$  is indicated in the visualization

$$d_{\text{edge}} = n_{\text{peri}} d_{\text{nozzle}} + \frac{v_{\text{infill}}^2 \sin\left(\alpha \frac{\pi}{180}\right)}{2a_{\text{max}}} \quad (1)$$

Here  $n_{\text{peri}}$  represents the number of specified perimeters,  $d_{\text{nozzle}}$  denotes the nozzle diameter,  $v_{\text{infill}}$  signifies the print speed under investigation,  $\alpha$  stands for the angle between the extrusion direction and the load direction, and  $a_{\text{max}}$  represents the maximum possible acceleration of the printer. It is assumed that the nozzle speed  $v_{\text{nozzle}}$  at the edge of the specimen, i.e., at the turning point, is  $v_{\text{nozzle}} = 0$  mm/s, which is considered conservative. Equation 1, alongside the process parameters detailed in Table 2, the specified specimen dimensions, the number of specimens, and the cutting width for cutting, results in the minimum plate sizes listed in Table 3. Five specimens were cut from the large plates. 5 mm of material was provided between each specimen for the separation process.

## 2.6 Tensile test

The tensile test was selected to achieve a uniaxial stress state, allowing for a clear interpretation of individual effects such as material orientation or failure mechanisms. A *Zmart Pro 200 kN* universal testing machine from *ZWICK/Roell*, equipped with a 20 kN load cell, was employed for testing. The specimens were clamped using hydraulic jaws featuring a finely ribbed surface. For precise strain evaluation using virtual extensometers, the commercial Digital Image Correlation (DIC) system *ARAMIS Adjustable* from *GOM Metrology GmbH*, with a recording frequency of 2 Hz, was utilized. The force signal from the testing machine was simultaneously integrated into the system. All experiments were performed at a room temperature of  $RT = 23$  °C.

## 2.7 Cutting methods

Water jet cutting (WJC) was selected for the initial investigations due to its capability to produce specimens of any geometry within the required tolerances. The potential influence of moisture on the mechanical properties of PLA resulting from the cutting process can be disregarded based on the short WJC process time and the findings of Banjo et al. [30]. To assess the impact of different cutting processes, laser cutting and milling were chosen in addition to WJC, as they can introduce additional influences on the specimens. Laser cutting subjects the specimens to direct thermal stress, whereas milling subjects them to mechanical stress.

### 2.7.1 Water jet cutting (WJC)

The *iCUT water smart* WJC system from *imes-icore* was utilized for the experiments. The manufacturer specifies

**Table 4** Parameters for water jet processing of additively manufactured PLA structures

Process parameter	Value	Unit
Nozzle speed $v_{\text{wj}}$	5	mm s <sup>-1</sup>
Pressure $p_{\text{wj}}$	1450	bar
Flow rate of cutting sand	250	g min <sup>-1</sup>

a positioning accuracy of 80  $\mu\text{m}^{-1}$  and a repeatability of less than 40  $\mu\text{m}^{-1}$ . Cutting sand, specifically *Classic Cut 120 garnet* from *GMA*, was employed as the cutting medium. The parameters employed for processing additively manufactured PLA structures are detailed in Table 4.

### 2.7.2 Laser cutting

The *Trotec Speedy 400* was used. A cutting study was performed to determine the lowest possible temperature effect on the specimens. The study resulted in process parameters corresponding to 100% of the adjustable power and 0.4% of the adjustable traverse speed.

### 2.7.3 Milling

A customized holder tailored to the specimen geometry was designed and manufactured for fixation in the milling machine. The milling process was executed in a total of six steps with the process parameters shown in Table 5:

1. Milling the outer contour with a tolerance of +0.15 mm to the nominal dimension in four steps, removing 1 mm of material at each step.
2. Precisely milling the contour to nominal dimensions over the full height of the specimen.
3. Sawing to the nominal length.

To prevent the specimen from heating up and the cutting edge from melting, water cooling was employed throughout all milling operations.

## 2.8 Micro-structure characterization

In various studies, both non-destructive methods like computer tomography [18, 31] or X-ray tomography [32, 33] and destructive methods are employed for microstructure characterization. In this work, the destructive method scanning electron microscopy (SEM) [18, 20, 24] was chosen as the preferred method. This decision was driven by the necessity to examine fracture surfaces in greater detail, in

**Table 5** Parameters for milling of additively manufactured PLA structures

Process parameter	Value	Unit
Feed rate $v_{fr}$	8	mm s <sup>-1</sup>
Milling head speed $p_{mh}$	13,000	R/min
Milling infeed	1	mm

addition to assessing the influence of cutting methods on the microstructure. The SEM analysis was conducted using a *LEO EVO 50* and a *LEO 1530* microscope from *Carl Zeiss AG*. The specimens were first cut to size, attached to a slide using conductive tape, and then sputtered with gold for 25 s at a voltage of 20 mV. To ensure sufficient conduction from the surface to the slide, a thin layer of conductive varnish was applied. The *LEO EVO 50* operated with an accelerating voltage of 20 kV, while the *LEO 1530* operated with an accelerating voltage of 5 kV.

### 3 Requirements and hypotheses

This work investigates the manufacturing of test specimens to represent the resulting structures within additively manufactured components accurately. This ensures that the structural properties of the component can be effectively characterized at the specimen level. To guarantee that the specimens faithfully reflect the structure to be tested and that no additional process-specific properties distort the structural properties, the following requirements for a representative specimen are defined and briefly explained:

**R 1** The process-related material orientation must be accurately replicated within the specimen according to the structure intended for investigation.

As demonstrated in numerous publications [6, 11–16, 18–20], material orientation significantly influences the resulting mechanical properties. Therefore, when characterizing these properties, it is crucial to ensure that specimen preparation does not distort the material orientation.

**R 2** A constant process speed must be maintained within the specimen test area to account for the influence of process speed fluctuations and the associated time interval between two deposited strands.

Hardware speed and acceleration limitations can lead to deviations from the nozzle speed specified in the slicer. Additionally, the time interval between the deposition of two adjacent strands can influence the degree of welding and, consequently, the resulting strength [18, 19].

**R 3** The uncertainty in specimen preparation with notable influence on characterization results should be minimized.

The resulting mechanical properties of additively manufactured structures can be sensitive to changing process conditions and external influences [6, 7]. Thus, uncertainties in printing and further processing of specimens may lead to fluctuating resultant properties that are not representative of the actual properties being tested.

In the following, hypotheses are formulated, and their validity is tested and evaluated within the scope of this publication to fulfill the above-mentioned requirements for a test specimen:

**H 1** Directly additively manufactured specimens involve non-constant process speed due to the printer-specific lower curve speed and acceleration after changes in trajectory direction.

**H 2** Directly additively manufactured specimens may exhibit an additional, unrepresentative material orientation due to the perimeter and the turning points of the deposited strands.

**H 3** By separating the specimens from a printed plate, the areas of turning points and lower printing speed are not present in the specimens. Thus, the effects formulated in **H 1** and **H 1** can be avoided.

**H 4** A dogbone specimen geometry results in more valid characterization tests compared to a rectangular geometry.

**H 5** The size of the printed plate used to produce the test specimens influences the mechanical properties and their uncertainty.

The hypotheses were investigated and evaluated based on tensile tests to assess the influence of process-related material orientation on mechanical properties, along with SEM images of fracture surfaces and cut edges.

## 4 Results and discussion

### 4.1 Comparison between directly printed and cut from plate

#### 4.1.1 Validity

To evaluate which specimen geometry and specimen preparation are more likely to result in valid tests and thus more effective characterization, the validity of the tests is recorded in addition to the mechanical properties, thereby checking **H 4**. This is achieved by verifying if the failure location is

within the valid gauge length of the specimen. The validity refers to minimum 10 tests performed. The results are depicted in Fig. 6, which has been partially presented in preliminary investigations in [26]. It is evident that only the dogbone geometry separated from the plate exhibits a clear majority of valid specimens for all tested material orientations.

The rectangular specimens fail outside the gauge length due to the stress jump at the clamps. The lower number of valid tests for the directly printed dogbone specimens can be attributed to the process-related notch in the area of the taper of the specimen width. Figure 7a illustrates the resulting notches and the local increase in strain during the tensile test. In comparison, Fig. 7b shows a homogeneous strain field during the test on a cut specimen. These findings are consistent with the observations of Park et al. [25]. Thus, the study demonstrates that a dogbone geometry increases the probability of valid tests, confirming H 4.

### 4.1.2 Fracture surface

Figure 8 displays SEM images of fracture surfaces of failed specimens with a material orientation of 90° as an example. The fracture surfaces of a directly printed specimen (a) and a cut specimen (b) are depicted. In the case of directly printed specimens, the material orientation of the perimeter is also tested rather than the actual material orientation intended for characterization. With an infill orientation of ±45°, the influence of the perimeter on the resulting fracture surface is similar. However, with a 0° orientation, the perimeter has no significant influence. These investigations thus confirm R 3. They demonstrate that this approach is essential for identifying potential failure mechanisms of an additively manufactured component structure without confounding effects from the perimeter or other edge effects.

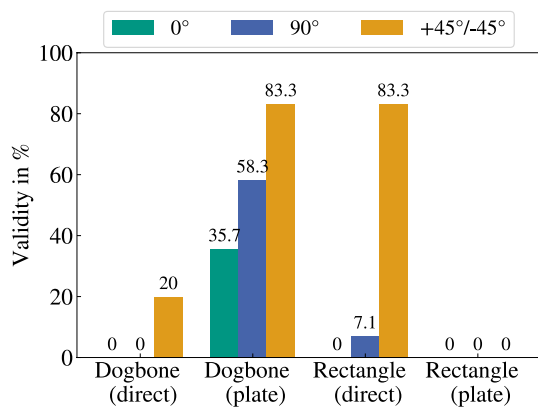


**Fig. 6** Validity of the tensile tests on rectangular and dogbone specimens directly printed (direct) and separated from the plates (plate). At least 10 tests were performed for each intralayer material orientation of 0°, 90° and ±45° to the loading direction

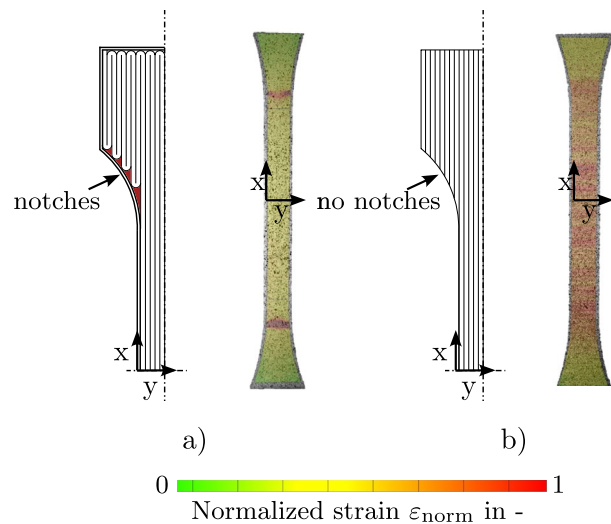


**Fig. 7** Directly printed specimen with notches (a) and cut specimen (b) with corresponding strain distributions during tensile test

### 4.1.3 Mechanical properties

The tensile tests exhibit linear elastic behavior. Figure 9 displays the mean tensile strength and mean stiffness resulting from the tensile tests initially presented in [26]. These tests were conducted on directly printed specimens and specimens cut from a large plate by WJC. Both valid and invalid tests were included to facilitate comparison between manufacturing methods. Overall, the influence of the preparation method on tensile strength is more pronounced than the influence on stiffness, particularly when the material orientation deviates from 0°.

*Tensile strength* The comparable tensile strength of the 0° specimens can be attributed to the non-critical influence of both the resulting notches (II in Fig. 10) and the additional 0° material orientations introduced by the perimeter (I in

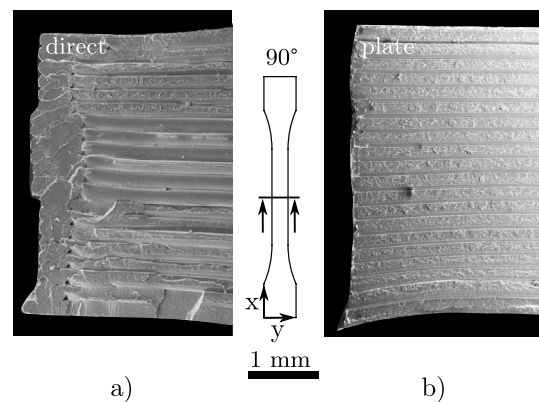


**Fig. 8** SEM images of the fracture surface of specimens with 90° material orientation. Shown is a directly printed specimen (a) and a specimen cut from a plate (b)

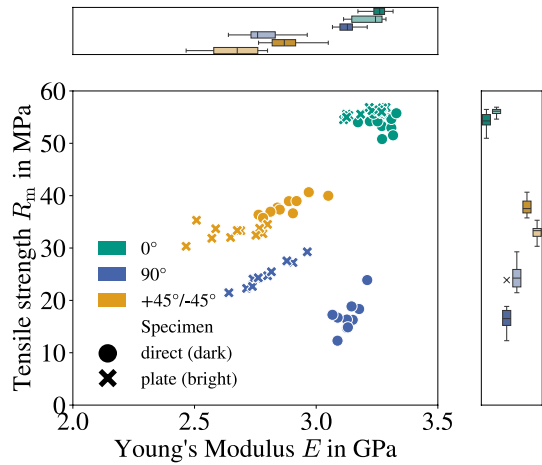


**Fig. 9** Results of tensile tests on directly printed (filled circle) and water jet-cut dogbone specimens from a large plate (times symbol) with intralayer material orientations  $0^\circ$ ,  $90^\circ$  and  $\pm 45^\circ$ . The measured values of each test and the standard deviation for the stiffness and strength of each configuration are shown. Initially presented in [26]

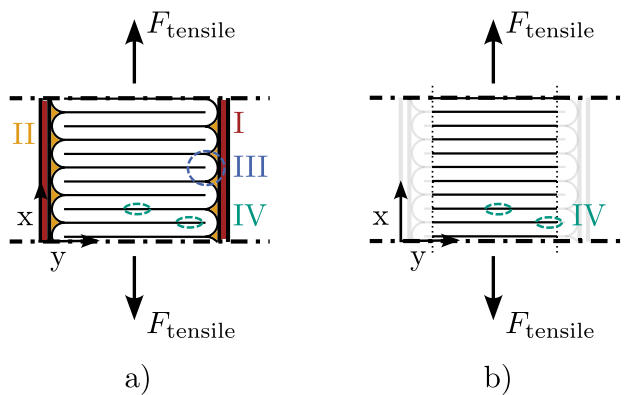


**Fig. 10** Schematic representation of the trajectory in the test area for a printed specimen (a) and a specimen cut from a plate (b). Colored highlighting and numbering of the expected effects based on the trajectory: The perimeter (I) introduces an additional material orientation. Notches (II) are formed by the turning points of the trajectory. Turning points (III) result in an additional material orientation along the load direction. Varying degrees of welding (IV) occur due to different times between the deposition of two adjacent strands at the turning point and in the center of the specimen

Fig. 10), turning points (III in Fig. 10), or blurred microstructure in the initial layers (Fig. 11). The lower strength of the directly printed specimen with a  $90^\circ$  material orientation is due to the process-related notches (Sect. 4.1.1). Therefore, it can be expected that the strength-reducing effect of these notches is greater than the strength-increasing effect of the additional  $0^\circ$  orientation. For this reason, the study did not include tests on directly printed specimens without a perimeter, as an even greater decrease in strength would be expected. For structures with a material orientation of  $\pm 45^\circ$ ,

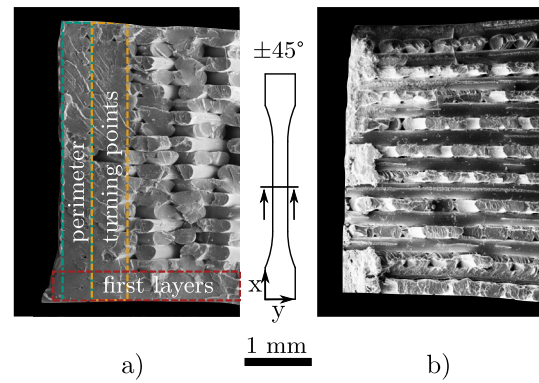


**Fig. 11** SEM images of the fracture surface of specimens with  $\pm 45^\circ$  material orientation. Shown is a directly printed specimen (a) and a specimen cut from a plate (b)

the strength of the directly printed specimens is higher. Because the shape of the dogbone specimen is more filled by the alternating  $+45^\circ$  and  $-45^\circ$  layers, the notches are less pronounced than with a  $90^\circ$  orientation. Therefore, the strength-reducing effect of the notches is less pronounced than the strength-enhancing effect of the additional  $0^\circ$  material orientations.

**Stiffness** The stiffness of the  $0^\circ$ -oriented structure is similar for both preparation types since the perimeter has the same material orientation as the orientation being tested. The higher stiffness of the  $\pm 45^\circ$ - and  $90^\circ$ -oriented structures with direct printing is attributed to the perimeter, as well as the turning points and thus the additionally integrated  $0^\circ$  orientation (I and III in Fig. 10). For  $\pm 45^\circ$  structures, the introduction of a  $0^\circ$  orientation has less influence on the resulting stiffness. Therefore, the difference in stiffness between the two preparation methods is less pronounced for  $\pm 45^\circ$  structures. To validate the influence of the perimeter on the resulting stiffness of a printed specimen, the resulting stiffness  $E_{\text{res}}^{\text{direct}}$  can be estimated from the measured stiffnesses of the cut  $0^\circ$  specimens  $E_0^{\text{plate}}$  and the corresponding orientation  $E_{\text{ori}}^{\text{plate}}$  using the mixing rule

$$E_{\text{res}}^{\text{direct}} = \phi E_{\text{ori}}^{\text{plate}} + (1 - \phi) E_0^{\text{plate}}. \quad (2)$$

where  $\phi$  denotes the fraction of the material orientation under analysis. The SEM image of the fracture surface of a directly printed  $\pm 45^\circ$  specimen in Fig. 11a illustrates the additional  $0^\circ$  orientation due to the perimeter, the turning points, and a blurring of the structure in the first layers. Conversely, Fig. 11b indicates that this blurring of the first layers is less pronounced in cut specimens. Assuming these areas possess the properties of a  $0^\circ$  oriented structure,  $\phi$  can be approximated as 0.635. This yields a modulus of elasticity of  $E_{\text{res}}^{\text{direct}} = 2.86$  GPa. Consequently, the plausibility check confirms that the perimeter, the turning points, and the blurring

of the microstructure in the area of the first layers impact the measured stiffness. Consequently, the measurement is not representative. These investigations confirm H 2.

*Scatter* The scattering is more pronounced in the cut specimens than in the directly printed specimens. Scattering can be caused by the effect labeled IV in Fig. 10. Owing to the turning point of the deposited strand, different times elapse between the deposition of two adjacent strands. In the area of the turning point, the times are shorter than in the center of the specimen or plate, which allows a higher degree of welding. This results in an inhomogeneous degree of welding across the cross section. In the case of directly printed specimens, the degree of welding is therefore not homogeneous across the cross section and does not represent the structural property being tested. However, the inhomogeneity is the same for all specimens, so the scatter is less pronounced. Although the use of plates avoids the effect of turning point acceleration described in Sect. 2.5, inhomogeneity of the degree of welding across the plate cross section remains. When multiple specimens are cut from a plate, this inhomogeneity is transferred to the specimens in the case of  $\pm 45^\circ$  and  $90^\circ$  structures. This can lead to a scattering of the measurement results. Therefore, in Sect. 4.2 the influence of the plate size and thus the influence of the preparation method on the measurement uncertainty is investigated.

### 4.2 Plate size

The influence of plate size is evaluated using the measured tensile strengths, stiffnesses, and their scatter as depicted in Figs. 12 and 13. As explained in Sect. 4.1.3, the plate size does not affect the mechanical properties of the  $0^\circ$  structure. Therefore, only the  $90^\circ$  and  $\pm 45^\circ$  material orientations will be discussed in this section. For this purpose, specimens are cut from two different plate sizes (Sect. 2.5). Since the same

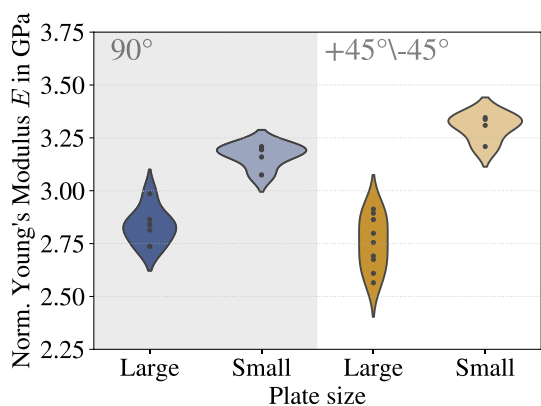


**Fig. 12** Young's modulus  $E$  normalized to the relative filling density  $\rho_{rel}$  for specimens cut from large plates and for specimens cut from plates from which exactly one specimen can be taken. Displayed as a violin plot [26]

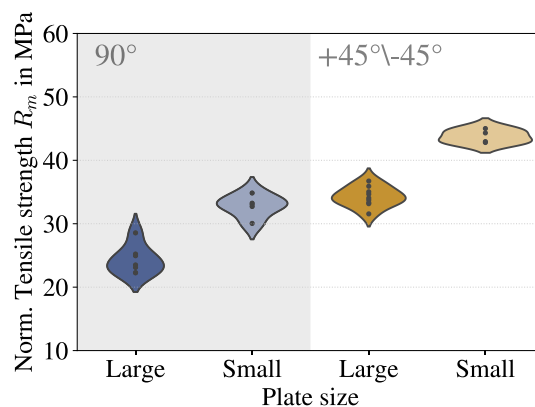


**Fig. 13** Tensile strength  $R_m$  normalized to the relative filling density  $\rho_{rel}$  for specimens cut from large plates and for specimens cut from plates from which exactly one specimen can be taken. Displayed as a violin plot [26]

orientations are being compared, only the influence on the degree of welding and its distribution over the cross-section of a specimen is considered. Therefore, the results are normalized to the relative filling density

$$\rho_{rel} = \frac{\rho_{specimen}}{\rho_{ref}} \tag{3}$$

This eliminates the influence of the printing process on the filling density. Density measurements were performed according to the Archimedean principle using the ME-DNY-43 density meter and the ME204T/00 analytical balance from Mettler Toledo. The density of the untreated filament, which was also measured, was used as a reference density.

This eliminates the influence of the printing process on the filling density. Density measurements were performed according to the Archimedean principle using the ME-DNY-43 density meter and the ME204T/00 analytical balance from Mettler Toledo. The density of the untreated filament, which was also measured, served as a reference density.

Both stiffness and tensile strength are greater and less scattered when the small plate is used. In particular, the stiffness scatter decreases significantly. The scatter arises from the heterogeneous interface properties across the width of the plate, as explained in Sect. 4.1.3. When only one specimen is cut from each plate, there is a consistent interface property among all specimens compared to the situation when multiple specimens are cut from a larger plate. An explanation for the higher measured mechanical properties is provided by Zhang et al. [24] and Vaes et al. [34]: For smaller specimens, less time elapses between the deposition of the individual strands adjacent to each other if the process parameters are kept constant. This further promotes

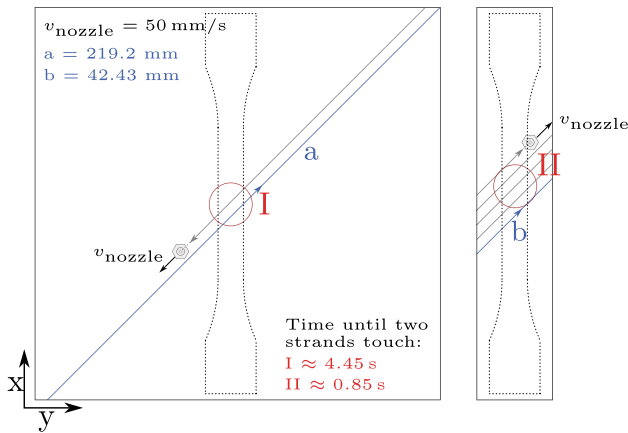


**Fig. 14** Schematic representation of the additively manufactured large and small plates with a dogbone specimen and the nozzle trajectory for a  $\pm 45^\circ$  material orientation. The time interval between the placement of two neighboring strands is indicated in red

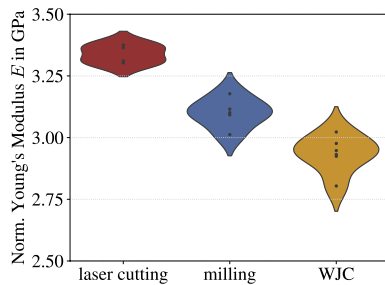


**Fig. 15** Young's Modulus  $E$  normalized to the relative filling density  $\rho_{rel}$  for specimens cut from small plates by WJC, milling, and laser cutting. Displayed as a violin plot

the welding of the strands and increases the load-carrying capacity. This effect is depicted in Fig. 14. Consequently, the choice of plate size influences the measured values and their uncertainty. Hypothesis H 5 stated in Sect. 3 is thus confirmed. To reproduce the actual structure to be tested independent of the plate size and thus meet Requirement R 1, it is necessary to set the time between the deposition of two adjacent strands according to the process conditions during component manufacture. This can be achieved by adjusting the G-code.

### 4.3 Influence of the cutting method

Dogbone specimens were cut from small plates by laser cutting, milling, and water jet cutting (WJC) and compared based on their mechanical properties using the  $90^\circ$  material orientation as an example. Figure 15 illustrates the stiffness normalized to the relative filling density  $\rho_{rel}$ , and Fig. 16 depicts the normalized tensile strength of these specimens.

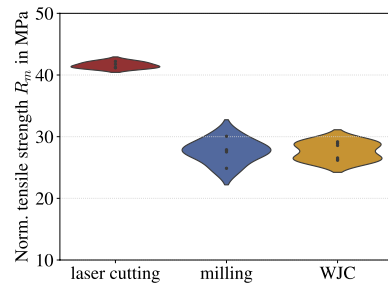


**Fig. 16** Tensile strength  $R_m$  normalized to the relative filling density  $\rho_{rel}$  for specimens cut from small plates by WJC, milling, and laser cutting. Displayed as a violin plot

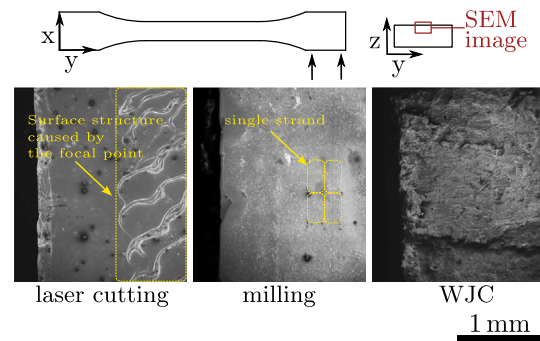


**Fig. 17** SEM images of the cut surface of laser cut, milled, and water jet cut specimens with a material orientation of  $90^\circ$ . The typical microstructure can be seen in the milled specimens (marked in yellow)

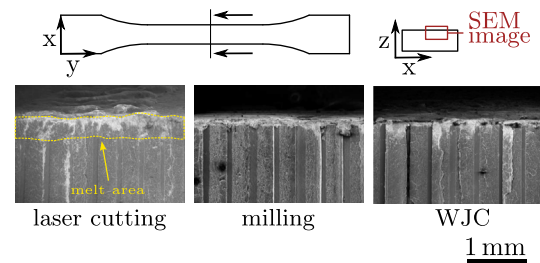


**Fig. 18** SEM images of the fracture surface of laser cut, milled and water jet cut specimens with a material orientation of  $90^\circ$ . The melt area created during laser cutting is highlighted in yellow

Both the stiffness and tensile strength of the laser-cut specimens are higher than those of the water jet-cut and milled specimens. This can be explained by the SEM images of the cutting edge and fracture surface shown in Figs. 17 and 18. As the cutting edges show, the edge zone melts during laser cutting. In particular, the laser focus in the center of the cutting edge leaves a characteristic surface structure. The fracture surface of a laser-cut specimen shows a layer-thick melted edge zone (marked in yellow in Fig. 18). This influence of the cutting method on the surface layer area is

not visible in milling and WJC and explains the increased mechanical properties. The slightly lower stiffness of the WJC specimens can be explained by the increasing width of the water jet. As a result, the cross-sectional shape is trapezoidal rather than rectangular and therefore slightly smaller than specified and more difficult to measure. In addition, WJC results in a much rougher surface with defects compared to laser cutting. The cut edge of a milled specimen has no significant effect on the edge area. The individual strands are visible (marked in yellow in Fig. 17). However, the defective surface of the WJC specimens has no significant effect on the measured tensile strength.

#### 4.4 Guidelines for specimen preparation

Based on the presented results, the following recommendations are made for test specimens to meet the requirements specified in Sect. 3:

##### *Specimen geometry*

- The investigations (Sect. 4.1.1) demonstrate that the specimen geometry significantly impacts the probability of valid tests, confirming hypothesis H 4. As a result, the dogbone geometry is recommended for test specimens.

##### *Transferring the component structure to coupon level*

- To ensure that the material orientation is accurately tested as intended (R 1), the specimen preparation must avoid introducing any deviating material orientation caused by the perimeter or turning points of the trajectory. Cutting the specimen from an additively manufactured plate prevents such deviations (Sect. 4.1), confirming hypotheses H 2 and H 3. Therefore, this method is recommended.
- To avoid acceleration paths within the measuring range (R 2), the time interval between the deposition of two adjacent strands must be constant over the entire specimen. This can be achieved by cutting the specimens from additively manufactured plates. Equation 1 can be utilized to ensure that there are no acceleration paths in the cut specimens.
- The time interval between two deposited strands must be transferred according to the process conditions during the manufacture of the component. This can be achieved by specifying a waiting time in the G-code before printing a strand.

##### *Cutting method*

- Milling preserves the typical MEX microstructure, avoids deviation from the specified cross-sectional shape, and is thus recommended as a cutting method. This

ensures compliance with R 3. The procedure outlined in Sect. 2.7.3 can be employed for this purpose.

##### *Reproducibility*

- The preparation method must remain consistent throughout a test series.
- All process parameters must be specified as shown in Table 2.
- To minimize the influence of the preparation method on measurement uncertainty, it is advisable to cut each specimen from a single plate. This approach ensures that the degree of welding is consistent across the cross-section of each specimen, thereby fulfilling R 3.
- It should be noted that the hardware and firmware installed in a printer can impact the printing outcome. Therefore, it is recommended to use the same printer consistently within a test series.

## 5 Summary and conclusions

The present work addresses the characterization of mechanical properties in components manufactured through Additive Manufacturing (AM) via Material Extrusion (MEX), focusing on the challenge of achieving consistent and reproducible results. Specifically, the research aims to identify the requirements for specimen preparation to accurately represent the distinctive structure of additively manufactured components at the coupon level. To address this challenge, the study formulates requirements for test specimens and hypotheses regarding their fulfillment. Various experimental investigations are conducted, evaluating preparation methods based on tensile strength, stiffness, intralayer material orientations ( $0^\circ$ ,  $90^\circ$ , and  $\pm 45^\circ$ ), and SEM imaging of fracture surfaces and cut edges. In conclusion, the main findings are:

- The comparison between directly printed dogbone specimens and those cut from a printed plate with rectangular geometry reveals that the cut dogbone specimens yield a higher number of valid tests.
- For material orientation in the direction of loading ( $0^\circ$ ), there are no significant differences in tensile strength and stiffness between directly printed and cut dogbone specimens.
- For specimens with material orientation transverse to the loading direction ( $90^\circ$ ), direct printing of the specimen results in higher stiffness due to the perimeter. However, the process-induced notches result in lower tensile strength.
- For specimens with  $\pm 45^\circ$  material orientation, direct printing of the specimen results in higher stiffness and

strength. The perimeter has a greater influence than the resulting notches.

- Especially for material orientations  $\pm 45^\circ$  and  $90^\circ$ , different plate sizes have an influence on the measured stiffness and strength as well as their scatter. An equation for dimensioning the plates is presented in this paper.
- Laser cutting as a cutting method leads to a fusion of the edge area and thus to an increase in stiffness and strength.
- Compared to milling, WJC results in an uneven surface with defects at the cut edge. However, this does not significantly affect the tensile strength. In addition, WJC results in a trapezoidal cross-section of the specimen, which makes it difficult to measure the cross-sectional area.

Finally, a guideline for the preparation of representative specimens is recommended: Dogbone specimens according to DIN EN ISO 527-2 should be used and milled from one plate. The plate size should be such that exactly one specimen can be taken. To ensure that the structure on the coupon level corresponds to the structure on a printed part, the time between the deposition of two adjacent strands must also be considered. Consistent definition of the process parameters leads to increased comparability and reproducibility of the results obtained. In further work, this preparation method can be further validated by producing a component with different local processing parameters and comparing the mechanical properties of corresponding specimens.

**Acknowledgements** The research documented in this manuscript has been funded by the German Research Foundation (DFG), project number 255730231, within the International Research Training Group “Integrated engineering of continuous-discontinuous long fiber reinforced polymer structures” (GRK 2078) and the Heisenberg Professorship of Prof. Kärger. The support by the German Research Foundation (DFG) is gratefully acknowledged. Furthermore, we thank the Baden-Württemberg Ministry of Science, Research and the Arts (MWK) for the funding of the project “Basics of a remanufacturing process chain for functional, hybridized polymer components to increase reusability and optimize resource utilization (Restore)” as part of the Innovation-Campus Future Mobility (ICM).

**Author's contributions** Conceptualization: Felix Frölich, Benedikt Scheuring, Anselm Heuer; Methodology: Felix Frölich, Benedikt Scheuring, Anselm Heuer; Formal analysis and investigation: Felix Frölich, Lennart Bechtloff, Benedikt Scheuring, Anselm Heuer; Writing—original draft preparation: Felix Frölich; Writing—review and editing: Lennart Bechtloff, Benedikt Scheuring, Anselm Heuer, Florian Wittemann, Luise Kärger, Wilfried V. Liebig; Funding acquisition: Luise Kärger, Wilfried V. Liebig; Resources: Wilfried V. Liebig; Supervision: Florian Wittemann, Luise Kärger, Wilfried V. Liebig.

**Funding** Open Access funding enabled and organized by Projekt DEAL. This study was funded by the German Research Foundation (DFG) (Grant No. 455807141) and the Baden-Württemberg Ministry of

Science, Research and the Arts (MWK). The authors have no relevant financial or non-financial interests to disclose.

**Data availability** The data generated in the context of this work are available from the corresponding authors upon reasoned request.

**Open Access** This article is licensed under a Creative Commons Attribution 4.0 International License, which permits use, sharing, adaptation, distribution and reproduction in any medium or format, as long as you give appropriate credit to the original author(s) and the source, provide a link to the Creative Commons licence, and indicate if changes were made. The images or other third party material in this article are included in the article's Creative Commons licence, unless indicated otherwise in a credit line to the material. If material is not included in the article's Creative Commons licence and your intended use is not permitted by statutory regulation or exceeds the permitted use, you will need to obtain permission directly from the copyright holder. To view a copy of this licence, visit <http://creativecommons.org/licenses/by/4.0/>.

## References

1. Huang Y, Leu MC, Mazumder J, Donmez A (2015) Additive manufacturing: current state, future potential, gaps and needs, and recommendations. *J Manuf Sci Eng Trans ASME* 137(1):1–10. <https://doi.org/10.1115/1.4028725>
2. Liu J, Gaynor AT, Chen S, Kang Z, Suresh K, Takezawa A, Li L, Kato J, Tang J, Wang CCL, Cheng L, Liang X, To AC (2018) Current and future trends in topology optimization for additive manufacturing. *Struct Multidiscip Optim* 57(6):2457–2483. <https://doi.org/10.1007/s00158-018-1994-3>
3. Singh S, Singh G, Prakash C, Ramakrishna S (2020) Current status and future directions of fused filament fabrication. *J Manuf Process* 55(January):288–306. <https://doi.org/10.1016/j.jmapro.2020.04.049>
4. Aliheidari N, Tripuraneni R, Ameli A, Nadimpalli S (2017) Fracture resistance measurement of fused deposition modeling 3D printed polymers. *Polym Test* 60:94–101. <https://doi.org/10.1016/j.polymertesting.2017.03.016>
5. Bellini A, Güçeri S (2003) Mechanical characterization of parts fabricated using fused deposition modeling. *Rapid Prototyp J* 9(4):252–264. <https://doi.org/10.1108/13552540310489631>
6. Cuan-Urquiza E, Barocio E, Tejada-Ortigoza V, Pipes RB, Rodriguez CA, Roman-Flores A (2019) Characterization of the mechanical properties of FFF structures and materials: a review on the experimental, computational and theoretical approaches. *Materials*. <https://doi.org/10.3390/ma12060895>
7. Montero M, Roundy S, Odell D (2001) Material characterization of fused deposition modeling (FDM) ABS by designed experiments. In: *Proceedings of rapid prototyping & manufacturing conference*, pp 1–21
8. Torrado Perez AR, Roberson DA, Wicker RB (2014) Fracture surface analysis of 3D-printed tensile specimens of novel ABS-based materials. *J Fail Anal Prev* 14(3):343–353. <https://doi.org/10.1007/s11668-014-9803-9>
9. Waseem M, Salah B, Habib T, Saleem W, Abas M, Khan R, Ghani U, Siddiqi MUR (2020) Multi-response optimization of tensile creep behavior of PLA 3D printed parts using categorical response surface methodology. *Polymers* 12(12):1–16. <https://doi.org/10.3390/polym12122962>
10. Khan I, Farooq U, Tariq M, Abas M, Ahmad S, Shakeel M, Riaz AA, Hira F (2023) Investigation of effects of processing parameters on the impact strength and microstructure of thick tri-material based layered composite fabricated via extrusion based additive

- manufacturing. *J Eng Res.* <https://doi.org/10.1016/j.jer.2023.08.007>
11. Hill N, Haghi M (2014) Deposition direction-dependent failure criteria for fused deposition modeling polycarbonate. *Rapid Prototyp J* 20(3):221–227. <https://doi.org/10.1108/RPJ-04-2013-0039>
  12. Tanikella NG, Wittbrodt B, Pearce JM (2017) Tensile strength of commercial polymer materials for fused filament fabrication 3D printing. *Addit Manuf* 15:40–47. <https://doi.org/10.1016/j.addma.2017.03.005>
  13. Penumakala PK, Santo J, Thomas A (2020) A critical review on the fused deposition modeling of thermoplastic polymer composites. *Compos Part B Eng.* <https://doi.org/10.1016/j.compositesb.2020.108336>
  14. Es-Said OS, Foyos J, Noorani R, Mendelson M, Marloth R, Pregar BA (2000) Effect of layer orientation on mechanical properties of rapid prototyped samples. *Mater Manuf Process* 15(1):107–122. <https://doi.org/10.1080/10426910008912976>
  15. Allum J, Gleadall A, Silberschmidt VV (2020) Fracture of 3D-printed micro-tensile specimens: filament-scale geometry-induced anisotropy. *Proc Struct Integr* 28(2019):591–601. <https://doi.org/10.1016/j.prostr.2020.10.069>
  16. Gao X, Qi S, Kuang X, Su Y, Li J, Wang D (2021) Fused filament fabrication of polymer materials: a review of interlayer bond. *Addit Manuf* 37(2):101658. <https://doi.org/10.1016/j.addma.2020.101658>
  17. Khan I, Tariq M, Abas M, Shakeel M, Hira F, Al Rashid A, Koç M (2023) Parametric investigation and optimisation of mechanical properties of thick tri-material based composite of PLA-PETG-ABS 3D-printed using fused filament fabrication. *Compos Part C Open Access* 12(August):100392. <https://doi.org/10.1016/j.jcomc.2023.100392>
  18. Heuer A, Huether J, Liebig WV, Elsner P (2021) Fused filament fabrication: comparison of methods for determining the interfacial strength of single welded tracks. *Manuf Rev.* <https://doi.org/10.1051/mfreview/2021031>
  19. Sun Q, Rizvi GM, Bellehumeur CT, Gu P (2008) Effect of processing conditions on the bonding quality of FDM polymer filaments. *Rapid Prototyp J* 14(2):72–80. <https://doi.org/10.1108/13552540810862028>
  20. Tao Y, Kong F, Li Z, Zhang J, Zhao X, Yin Q, Xing D, Li P (2021) A review on voids of 3D printed parts by fused filament fabrication. *J Mater Res Technol* 15:4860–4879. <https://doi.org/10.1016/j.jmrt.2021.10.108>
  21. Ahn SH, Montero M, Odell D, Roundy S, Wright PK (2002) Anisotropic material properties of fused deposition modeling ABS. *Rapid Prototyp J* 8(4):248–257. <https://doi.org/10.1108/13552540210441166>
  22. DIN Deutsches Institut für Normung e. V (2012) DIN EN ISO 527-2:2012, plastics—determination of tensile properties—part 2: test conditions for moulding and extrusion plastics. Beuth Verlag GmbH, p 14
  23. Laureto JJ, Pearce JM (2018) Anisotropic mechanical property variance between ASTM D638-14 type I and type iv fused filament fabricated specimens. *Polym Test* 68(April):294–301. <https://doi.org/10.1016/j.polymertesting.2018.04.029>
  24. Zhang Y, Choi JP, Moon SK (2021) Effect of geometry on the mechanical response of additively manufactured polymer. *Polym Test.* <https://doi.org/10.1016/j.polymertesting.2021.107245>
  25. Park SJ, Lee JE, Jin SC, Lee NK, Choi K, Park SH, Son Y (2022) Tensile test of additively manufactured specimens with external notch removed via laser cutting in material extrusion. *Polym Test* 110(April):107581. <https://doi.org/10.1016/j.polymertesting.2022.107581>
  26. Frölich F, Bechtloff L, Scheuring BM, Heuer AL, Kärger L, Liebig WV (2023) Development of a test method for characterization of the orientation dependent material properties of FFF structures. In: 23rd international conference on composite materials (ICCM 2023), Belfast. <https://doi.org/10.5445/IR/1000161267>
  27. BASF 3D printing solutions: technical data sheet ultrafuse PLA. Technical report (2020). Accessed: 2024-01-30
  28. Baran EH, Yildirim Erbil H (2019) Surface modification of 3d printed PLA objects by fused deposition modeling: a review. *Colloids Interfaces.* <https://doi.org/10.3390/colloids3020043>
  29. Knirsch J, Frölich F, Hof L, Wittemann F, Kärger L (2024) pyGCodeDecode: A Python package for time-accurate GCode simulation in material extrusion processes. *J Open Source Softw* (submitted)
  30. Banjo AD, Agrawal V, Auad ML, Celestine ADN (2022) Moisture-induced changes in the mechanical behavior of 3D printed polymers. *Compos Part C Open Access* 7:100243. <https://doi.org/10.1016/j.jcomc.2022.100243>
  31. Englert L, Heuer A, Engelskirchen MK, Frölich F, Dietrich S, Liebig WV, Kärger L, Schulze V (2022) Hybrid material additive manufacturing: interlocking interfaces for fused filament fabrication on laser powder bed fusion substrates. *Virtual Phys Prototy* 17(3):508–527. <https://doi.org/10.1080/17452759.2022.2048228>
  32. Nogales A, Gutiérrez-Fernández E, García-Gutiérrez MC, Ezquerro TA, Rebolgar E, Šics I, Malfois M, Gaidukovs S, Gäe Cis E, Celms K, Bakradze G (2019) Structure development in polymers during fused filament fabrication (FFF): an in situ small- and wide-angle X-ray scattering study using synchrotron radiation. *Macromolecules* 52(24):9715–9723. <https://doi.org/10.1021/acs.macromol.9b01620>
  33. Shmueli Y, Lin YC, Lee S, Zhernenkov M, Tannenbaum R, Marom G, Rafailovich MH (2019) In situ time-resolved X-ray scattering study of isotactic polypropylene in additive manufacturing. *ACS Appl Mater Interfaces* 11(40):37112–37120. <https://doi.org/10.1021/acsami.9b12908>
  34. Vaes D, Coppens M, Goderis B, Zoetelief W, Van Puyvelde P (2021) The extent of interlayer bond strength during fused filament fabrication of nylon copolymers: an interplay between thermal history and crystalline morphology. *Polymers.* <https://doi.org/10.3390/polym13162677>

**Publisher's Note** Springer Nature remains neutral with regard to jurisdictional claims in published maps and institutional affiliations.